

ALBERT-LUDWIGS-UNIVERSITÄT FREIBURG

MASTER THESIS

Readout of Wavelength-shifting Optical Modules

Author:

Johannes ALT

Supervisor:

Prof. Dr. Horst FISCHER

February 8, 2023



Fakultät für Mathematik und Physik

Abstract

The SHiP experiment is a proposed beam dump experiment to be built at the SPS to study physics beyond the Standard Model. To meet SHiP's zero background requirement, the Sourrunding Background Tagger (SBT) encloses the hidden sector decay volume. The SBT is a large-scale structure consisting of around 2000 cells filled with the liquid scintillator LAB. In each cell, two Wavelength-shifting Optical Modules collect the scintillation light and guide it to an array of SiPMs. The charge signals from the SiPMs are further amplified and digitized. During this thesis, a readout for usage with a prototype of one of the cells was assembled and commissioned. The readout consists of two main parts: a breakout board that can be plugged into the back of the SiPM PCB and uses the eMUSIC chip as an amplifier and shaper and GANDALF modules, which digitize the amplified output signals from the eMUSIC. This thesis investigated operation parameters of the eMUSIC chip. For the use of two GANDALFs, an external clock was developed and the GANDALF firmware was modified to enable the self-triggering of input signals with positive signal polarity.

Zusammenfassung

Das SHiP Experiment ist ein vorgeschlagenes Beam-Dump Experiment welches an dem SPS aufgebaut werden soll um Physik jenseits des Standard Models zu erforschen. Um SHiP's Anspruch, keinen Hintergrund zu haben, zu erfüllen, wird das Hidden Sector Zerfallsvolumen von dem Sourrunding Background Tagger (SBT) umgeben. Der SBT ist eine große Konztruktion aus etwa 2000 Zellen, welche mit dem Flüssigszintillator LAB gefüllt werden. In jeder Zelle befinden sich zwei Wavelength-shifting Optical Modules (WOM) um das Szintillationslicht einzufangen und zu einem Array von SiPMs geführt. Die Ladungssignale der SiPMs werden weiter verstärkt und digitalisiert. In dieser Arbeit wurde eine Auslese für einen Prototypen einer der Zellen zusammengestellt und in Betrieb genommen. Die Auslese besteht aus zwei Hauptteilen: einem Breakout-Board, welches auf die Rückseite der SiPM Platine gesteckt werden kann und den eMUSIC Chip als Verstärker und Shaper benutzt und GANDALF Modulen, welche die Verstärkten Signale digitalisieren. Im Rahmen der Arbeit wurden Betriebsparameter des eMUSIC Chips untersucht. Für die Benutzung von zwei GANDALFs wurde eine externe Clock entwickelt und die GANDALF Firmware wurde modifiziert um das Selbsttriggern auf Signale mit positiver Signalpolarität zu ermöglichen.

Contents

1	Introduction	3
2	One Cell Prototype	7
2.1	The Cell & Liquid Scintillator	7
2.2	Wavelength-shifting Optical Module & Optical Coupling	9
2.3	Silicon Photomultiplier	10
2.4	The eMUSIC board	13
2.5	The Generic Advanced Numerical Device for Analytic and Logic Functions (GANDALF) Module	19
2.5.1	Input Mezzanine Cards	19
2.5.2	GIMLI Mezzanine Cards	21
2.5.3	Usage of the GANDALF with Silicon Photomultipliers (SiPMs)	21
3	Setup	23
3.1	SiPM	23
3.2	Dark Box Setup	25
3.3	Gandalf	27

4 Results of the DAQ Tests	29
4.1 GANDALF Clock Frequency and ADC Test	29
4.2 Input Offset Voltage	31
4.3 Pole-Zero Cancellation Shaper	37
4.4 Transimpedance and Pole-Zero Attenuation	41
4.5 Dark Count Measurements	44
5 DAQ Performance at the DESY Testbeam	47
6 Summary and Outlook	49
A List of acronyms	51
List of Figures	53
List of Tables	55
Bibliography	56

Chapter 1

Introduction

So far, the best physical description of particle physics is provided by the Standard Model of particle physics (SM). However, through observations of different phenomena, which the SM can not explain, like neutrino oscillation [1, 2] and observations related to so called Dark Matter or Dark Energy [2], it is known that the SM can not be a complete theory []. Therefore different experiments are in development or are operating to search for new physics and particles outside the SM. One possible future experiment to join the search for new physics is the proposed Search for Hidden Particles (SHiP) experiment. It is an intensity frontier experiment using the 400 GeV proton beam from CERN’s Super Proton Synchrotron (SPS) and dumping it into a fixed target in order to observe rare events. SHiP is planned to be a zero background experiment to detect these rare events. It searches for long-lived heavy neutral particles from the so-called Hidden Sector (HS), for example, heavy right-handed leptons, dark photons, and light dark matter [3].

Figure 1.1 shows the proposed setup of SHiP. The 400 GeV protons get dumped into a high-density target, for example, a target out of tungsten. In the interaction between the protons and the target nucleons, SM particles and HS particles can be produced. In order to remove the SM particles, two kinds of shielding are used: The first one is a hadron absorber which is placed behind the target to absorb produced hadrons and electrons. Thereafter, magnetic muon shield deflects the muons to the side and out of the direction of the decay volume. So only neutrinos and HS particles remain. Behind the muon shield a neutrino and scattering detector is



Figure 1.1: Overview of the proposed setup for the SHiP experiment. The target on the left is used as a beam dump for the SPS. Most SM particles get absorbed by the hadron absorber directly behind the target. A magnetic muon shield deflects the muon, which will not be absorbed by the hadron absorber, away from the beam line. After the muon shield is a scattering and neutrino detector, and afterward, the 50 m long decay volume in which non SM particles created at the target can decay into SM particles. Behind the decay volume, the decay spectrometer is placed. To achieve the zero background goal, the Surround Background Tagger mounted around the decay volume plays a crucial role. [4]

placed to study neutrino physics cases. The next part is the HS decay volume. It is a 50 m long vacuum chamber in which the HS particles can decay into SM particles. The decay products then get detected in the HS decay spectrometer behind the HS decay volume. With the data produced by the HS decay spectrometer, the events can get reconstructed. From the measurements taken by the HS decay spectrometer, the long lived neutral particle can get reconstructed.

One problem for the measurement can be caused by SM particles entering the decay volume, falsely reconstructed as HS events in the spectrometer. Such a background can be muons deflected by the muon shield, reflected at the walls of the facility back into the decay volume, mimicking the decay products of an HS event in the spectrometer. It is crucial for background suppression to detect charged particles entering the decay volume and to tag them as background. This task is meant to be done by the Surrounding Background Tagger (SBT). As the name suggests, it surrounds the HS decay volume, detecting particles entering it. It is currently in development and this thesis is part of the R&D effort toward it. In the following, the SBT and the principles of the different parts are described. The details of the

different parts important for this thesis are presented in more detail in the next chapter.

To make the tagging of background events as efficient and pure as possible and to avoid the false tagging different pieces of information need to be known about the particles entering the decay volume. These pieces of information are the energy loss, the time and the space coordinates at which the particles enter the HS decay volume. Therefore the SBT is designed as a five-dimensional tagger. The five dimensions are the time when which the particle moves through the SBT, the three space coordinates where the particle enters the decay volume and the energy loss of the particle in the SBT. The SBT will consist of approximately 2000 cells that form the walls on the side as well as the top and bottom of the vacuum decay chamber. The structure is shown in Figure 1.2a. In order to fit the overall truncated pyramidal shape of the decay volume, the cells have an unsymmetric shape, an example is shown in Figure 1.2b. Both of the long edges are parallel, but the shorter sides are not. The depth of the cells is 25 cm and the wall thickness is planned to be 2 cm [4]. For the detection of particles, a liquid scintillator will be filled into the cells. A particle passing through one or more cells will deposit energy in the scintillator, causing scintillation light. The amount of emitted light is correlated to the amount of energy deposited in the scintillator. Two Wavelength-shifting Optical Modules (WOMs), PMMA tubes coated with wavelength-shifting paint, are placed in each cell to collect the scintillation light and guide it to an array of SiPMs. The signals from the SiPMs can be amplified, digitized, and further processed. Both a WOM and a SiPM array are shown in Figure 1.2c.

This thesis is in the scope of the R&D of the SBT. For the R&D of the SBT, a prototype of one of the cells was built, with which important parts can be tested. Starting from the cell's material itself, a reflecting coating on the inside of the cell, the WOM vessel, the coated WOMs, the SiPMs and the optical coupling and the readout electronics, to name only a few. This thesis is about the readout of the WOMs of this prototype. In the long run a dedicated Application Specific Integrated Circuit (ASIC) will be used for the readout of the SBT. However, since this chip is still in a very early stage of development by the Forschungszentrum Jülich a readout of the shelf is used for the One Cell Prototype in order to test it. The next chapter presents the One Cell Prototype with a focus on the WOM readout.

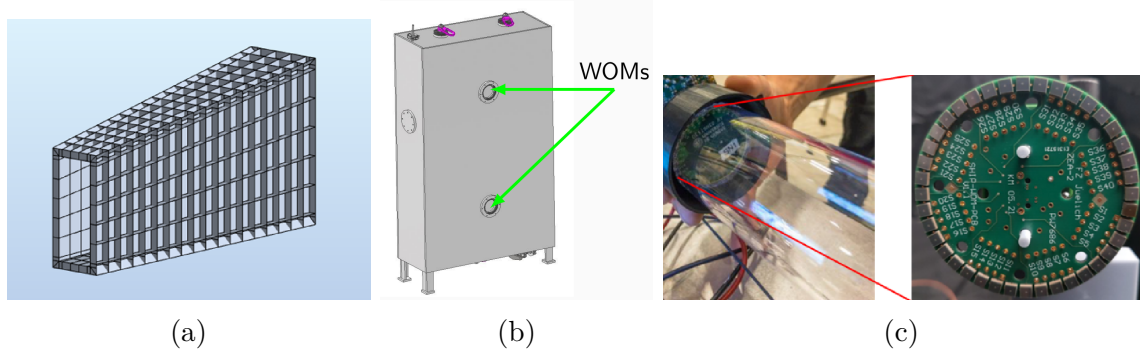


Figure 1.2: The structure of the Surrounding Background Tagger (SBT). Left is the SBT with approximately 2000 cells [5]. Then the prototype of one example cell is shown in b) [6]. The light produced by the liquid scintillator inside the cells is captured by two Wavelength-shifting Optical Modules (WOMs) per cell, an example is shown in c) [], and then guided to an array of Silicon Photomultiplier which will detect the light.

Chapter 2

One Cell Prototype

The work presented in this thesis is done in the framework of the so called “One Cell Prototype”. Therefore the prototype is described in more detail in this chapter. Although the important parts of the One Cell Prototype are all mentioned here, the main focus lies on the amplifier and the digitizer since these are the most relevant parts of this thesis. Firstly the cell and the liquid scintillator are shown, followed by the WOM used to capture the scintillation light, the SiPMs used for the light detection, and the optical coupling between the WOM and the SiPMs, are presented afterward. Subsequently, the amplifier and the digitizer are introduced.

2.1 The Cell & Liquid Scintillator

In Figure 2.1a, the One Cell Prototype is shown. It is a 80 cm wide and around 120 cm high container. The precise height depends on the position in the cell due to the asymmetric shape. The walls of the container consist of 1 cm thick corten steel. The steel was chosen to minimize the SBTs mass, which is an important aspect considering its size [4]. A thickness of 1 cm is only half of the planned 2 cm wall thickness of the SBT design. The SBT needs such thick walls in order to withstand the vacuum on the inside. For the R&D with the One Cell Prototype, the thickness was reduced to be able to perform measurements with different wall thicknesses by adding steel plates to the outside. This is important in case the SBT design



Figure 2.1: The One Cell Prototype at the DESY testbeam area a) and a PMMA vessel with a Wavelength-shifting Optical Module inserted and a SiPM board attached b). []

changes, for example by replacing the vacuum with helium. One side of the cell has two holes with equal distance to both side walls. The lower hole is 30 cm away from the bottom of the cell, and the upper hole is 30 cm below the top. In each of these holes, a PMMA vessel, shown in Figure 2.1b, is placed to house the two WOMs. Through an air gap between the WOMs and the PMMA vessel walls the photons in the WOMs are captured there by total reflection at the WOM air interface.

The container is filled with Linear Alkyl Benzene (LAB) mixed with $2\frac{g}{L}$ Diphenyloxazole (PPO)A UV reflective paint was applied to the inside of the container to increase the scintillator's light yield and therefore increase the detector's efficiency. In order to allow decompression and compression by temperature change, an expansion vessel is mounted on top of the cell. The cell was overfilled with scintillator, in order to still being full if the temperature declines and the scintillator compresses. Gaseous nitrogen fills out the remaining volume of the expansion vessel to avoid contact to air and to serve as a compressible volume.

2.2. WAVELENGTH-SHIFTING OPTICAL MODULE & OPTICAL COUPLING9

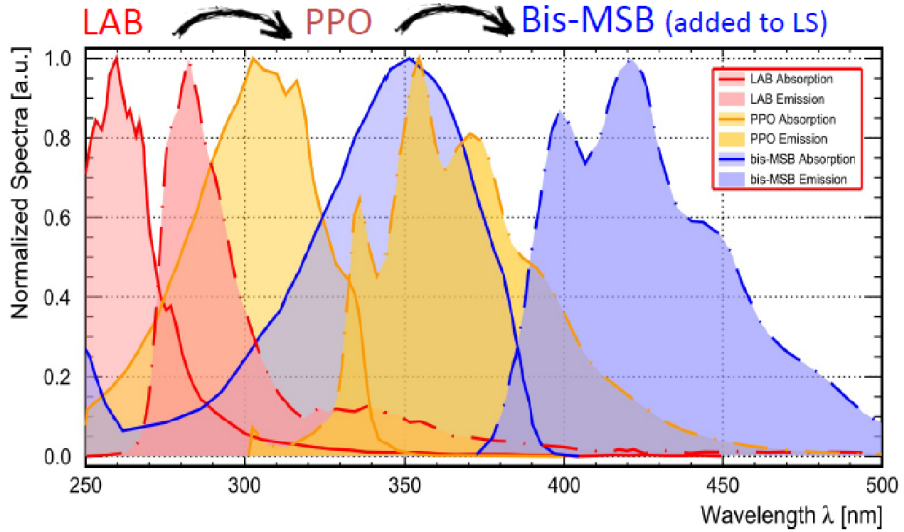


Figure 2.2: The emission spectrum of the liquid scintillator components LAB and Diphenyloxazole (PPO) and the wavelength shifter Bis-MSB. []

The LABs emission spectrum is shown in Figure 2.2. Most of the scintillation light has a wavelength of 320 nm to 360 nm. In order to capture the light and to shift the wavelength towards values for which the used SiPMs have a higher detection efficiency, WOMs are used. In the next section, these WOMs and the optical coupling between them and the SiPMs are presented.

2.2 Wavelength-shifting Optical Module & Optical Coupling

So-called WOMs are used to capture the scintillation light. They are PMMA cylinder walls with a 6 cm outer diameter and a 3 mm wall thickness. The design and material choice both make the cost of the light collection relatively cheap. Both the inside and outside of the PMMA cylinder are coated with the wavelength shifter Bis-MSB [7]. So the captured photons are shifted to a larger wavelength, for which the SiPMs used have a higher efficiency. Figure 2.2 shows the wavelength spectrum of the wavelength-shifted light. The photons which enter the WOM are trapped there by total reflection on the walls. They can leave the WOM at its end, where an array of SiPMs can detect them. For a good optical coupling between the WOM

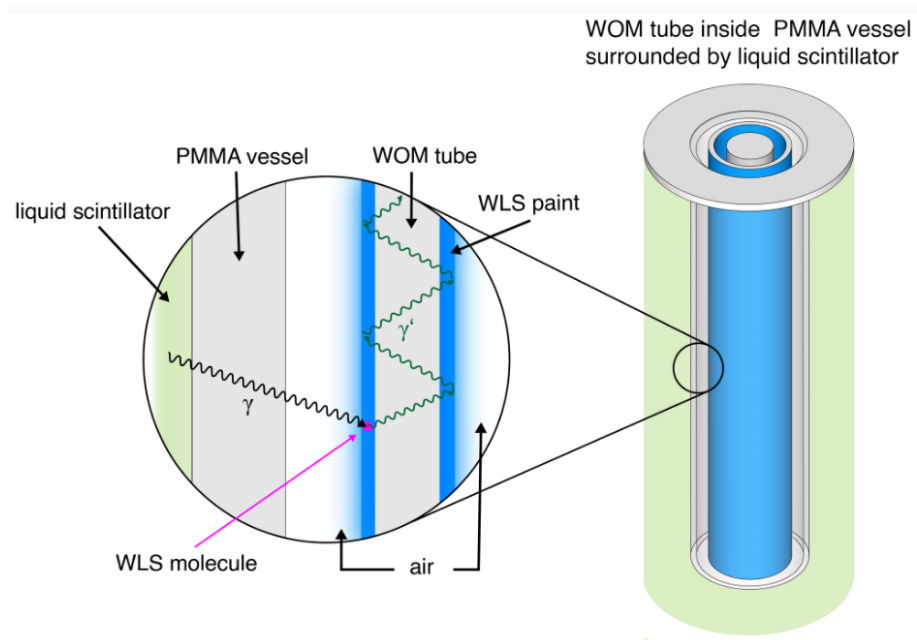


Figure 2.3: A wavelength-shifting optical module (WOM) is a PMMA tube coated with the wavelength shifter Bis-MSB. When a photon in the UV range hits the WOM, its wavelength gets shifted. Afterward, in the WOM, the photon is trapped by total reflection. At the end of the WOM, the photon can be detected by a photosensor. [8]

and the SiPMs, either optical grease or silicon pads can be used. Figure 2.3 illustrates the principle of the WOM with the wavelength shifting and capture by total reflection.

In the next part, the SiPMs, which detect the light captured by the WOMs, are presented.

2.3 Silicon Photomultiplier

In order to correctly identify and tag background events, the light detection of the SBT has to provide accurate timing information. Furthermore, due to the large number of cells and WOMs in the SBT, cost optimization is essential. To fulfill both requirements, SiPMs were chosen as photodetectors. These photodetectors consist of up to thousands of pixels [9].

Each pixel in the SiPM is an Single Photon Avalanche Diode (SPAD), which is a Avalanche Photodiode (APD) supplied with a voltage greater than its breakdown voltage [10]. In the following, the principle of such an APD and SPAD are explained.

Similar to every photodiode, APD utilize, the photoelectric effect to generate an electric charge signal in response to a light signal. They consist of doped silicon. An example is shown in Figure 2.4. It has a strongly n-doped layer, followed by a strongly p-doped layer, an intrinsic, weakly p-doped layer, and another p-doped layer. By adding the intrinsic layer, the region in which the photons can be absorbed increases. It generates an electron-hole pair, when a photon gets absorbed. When a reversed bias voltage is applied, the electric field in the APD separates the *eh*-pair. In case the APD is operated in the Geiger mode, meaning the bias voltage is higher than the breakdown voltage of the APD, the electric field at the strongly doped *p*- and *n*-layer is sufficiently high, that a self-sustaining avalanche is triggered by either the electron or the hole moving through it. Then the APD is called SPAD. The macroscopic signal of a SPAD makes it possible to detect single photons [11]. In order to stop the avalanche, a quenching resistor is connected in series to the SPAD [9]. With an increasing current signal flowing through the quenching resistor, the voltage drop at this resistor increases, and thus the bias voltage at the SPAD decreases. When the bias voltage drops below the breakdown voltage, the avalanche is no longer self-sustaining and stops. Thus the signal amplitude of a SPAD is always similar, independent of how many photons arrive at the same moment.

In SiPMs, hundreds to thousands of SPADs are connected in parallel, each with a high-resistance quenching resistor in series. Usually, the SPAD pixels are placed in a rectangular form with an edge length of a few mm. Due to the property of the SPADs that the output signal is always similar for each SPAD, the output signal of a SiPM is the output signal of one SPAD multiplied by the number of triggered SPADs. Therefore, if the number of photons arriving simultaneously at a SiPM is low enough that the probability of one SPAD being hit by two or more photons is low, one can count photons with a SiPM [9]. This and the relatively low cost of around 450 000 € for 100 000 SiPMs , high durability, and immunity to magnetic fields [9, 13] makes SiPM a good choice for photodetection for the SBT and similar detectors. However, due to the sensitivity down to single photons, also *eh*-pairs created by thermal excitation will cause signals indistinguishable from signals caused



Figure 2.4: Composition of an avalanche photodiode with the bias voltage V_B applied in the reverse direction. Between the contact to the ground and the strongly doped n^+ layer is the quenching resistor R_q connected in series. Next to the n^+ layer is a strongly doped p^+ layer. In the region of these two layers is the electric field, shown in the right figure, the strongest. There, an electron or hole can initiate an avalanche. After the p^+ layer is an intrinsic weakly doped π layer. This layer increases the sensitive volume of the diode. If an electron-hole pair is created, it gets separated by the electric field. The hole drifts towards the multiplication region and can start an avalanche. The next layer is a p^+ layer, which connects to a metal connector and high voltage. The picture in the middle illustrates the number of donators n_D and acceptors n_A , and the last picture illustrates the field strength at the different regions of the APD. [12]

by photons. These signals are called Dark Count (DC).

An essential property of a SiPM is the gain G . It describes the number of charge carriers released in each avalanche. Due to the quenching, this parameter is well-defined [10]. It can be calculated from the applied voltage V_{bias} , the breakdown voltage V_{bd} and the capacitance C_d of a SPAD with

$$G = \frac{(V_{\text{bias}} - V_{\text{bd}}) \cdot C_d}{e} [11]. \quad (2.1)$$

Here, e represents the charge of one electron. Usually, the gain is in the order of 10^5 to 10^7 [9]. Since the breakdown voltage of different SiPMs of the same model can differ slightly, also the gain with the same bias voltage can differ. The temperature also influences the breakdown voltage and the gain [13].

The next section presents an ASIC used to further amplify the SiPM signals before they can be digitized for electronic storage.

2.4 The eMUSIC board

Since the signals of the SiPMs are tiny, they need to be further amplified. For this purpose, the enhanced Multiple Use SiPM IC for photodetector readout (eMUSIC) ASIC by Scientifica [14] was chosen, and a custom Printed Circuit Board (PCB) housing the eMUSIC ASIC, from here on called eMUSIC board, was designed by the electrical engineers of the University of Freiburg. In the following first, the ASIC itself and afterward, the eMUSIC board will be presented.

The eMUSIC ASIC was developed by Scientifica for the readout of SiPMs. It comprises amplification, shaping and digital triggering. A block diagram for the ASIC is shown in Figure 2.5. It has eight input channels, each equipped with a $\approx 1\text{V}$ anode voltage control to equalize the overvoltage between the different channels. Because the SiPM is a charge source, each channel has a current mode input stage. The eMUSIC ASIC was designed for a low input transimpedance but provides the option of a high transimpedance mode with which the effective gain can be increased. Each channel has an analog bandwidth of 150 MHz and is equipped with a pole-zero cancellation. The schematics of the later is shown in Figure 2.6.

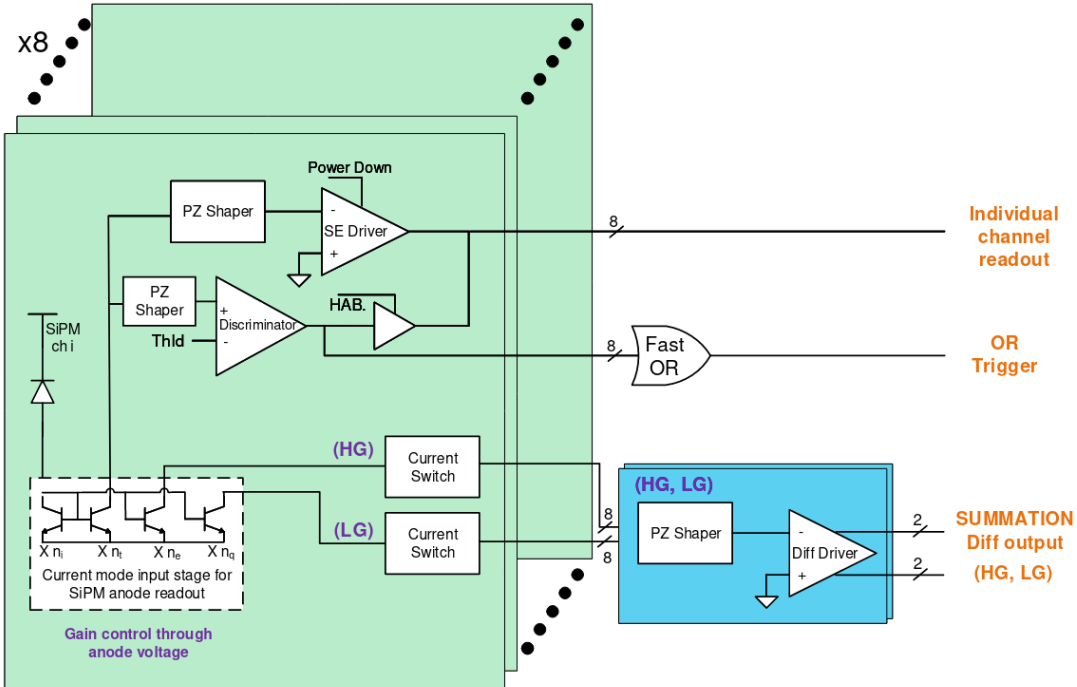


Figure 2.5: The block diagram of the eMUSIC ASIC. At the input is the current mode input stage, which can also set an offset voltage on the input to adjust the overvoltage channel by channel. The signal is shaped by the pole-zero cancellation shaper and amplified and can be read out for each channel as a single-ended signal. The discriminator can set a threshold to create a digital signal which can be read out channel by channel instead of the analog output signal. A fast OR output can also be used to put out a digital OR of all eight discriminator outputs. With the summation outputs, one can put out the sum of an arbitrary set of channels with two gains as differential signals. [15]

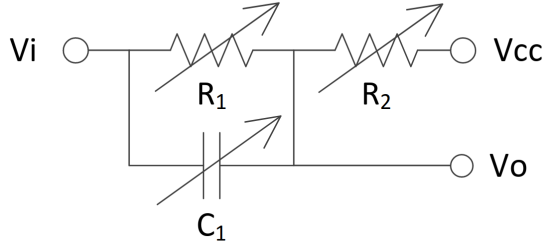


Figure 2.6: Sketch of a pole-zero cancellation with adjustable resistors and capacitor, the input voltage V_i , the output voltage V_o , and the operation voltage V_{cc} . [15]

The pole-zero cancellation is comprised of two adjustable resistors and an adjustable capacitor and can be used to decrease the Full Width at Half Maximum (FWHM) of the output signal to below 10ns. However, a smaller width also decreases the amplitude of the signal. The resistor has eight possible values it can be set to, and the capacitor has thirty-two different steps. A compromise between shorter signals and higher amplitude should be chosen depending on one's needs. Alternatively, the pole-zero cancellation can be disabled completely, resulting in the highest signal amplitude possible but also in the longest signal. The shaper outputs are connected to an analogue output for each channel.

Each channel is equipped with a discriminator with an adjustable threshold to form a channel-by-channel trigger signal. These logical signals can be either put out by using the individual output of the channel for the digital signal instead of the analog waveform or by using the fast OR of all channels. This fast OR allows, for example, the external triggering of the digitizer, which then digitizes the analog waveforms. The dynamic range of the output for the single-ended signals is 1 V if the load on the output is 50Ω and 2 V if a high impedance load is used on the output. Using the low transimpedance mode, the gain of the single-ended output is 180Ω , and with the high transimpedance mode, it is 480Ω . The response of the eMUSIC is linear only in its first half of the dynamic range.

Besides the individual readout of the eight channels, the eMUSIC can sum up the signal of an arbitrary set of channels with both high and low gain and put them out via two differential outputs. The bandwidth of this summation output is 500 MHz, and the output range is 1.25 V. Depending on whether the high or low transimpedance

is used, the gain of the high gain summation is 690Ω or 90Ω and 315Ω or 45Ω for the low gain summation. The response of the summation output is linear over the entire dynamic range.

Besides choosing the channels for summation, also each of the eight single-ended outputs can be individually turned on and off. Another important option that can be configured is the adjustment of the output DC offset to maximize the rail-to-rail voltage swing.

The trigger threshold for the digital outputs can be set with two parameters. The first one is the bandgap voltage V_{bg} of the comparators, which can be adjusted in eight steps between 487.22 mV and 2436.8 mV. The second parameter sets the Digital to Analog Converter (DAC) value N_{DAC} for the comparators. It can be set to DAC counts from 0 to 511. The finer threshold steps V_{fine} can be calculated with

$$V_{fine} = 1637.79 \text{ mV} - N_{DAC} \cdot 3.1445 \text{ mV}. \quad (2.2)$$

With V_{bg} and of V_{fine} or N_{DAC} , the final threshold

$$V_{th} = 1.5 \cdot V_{bg} - 0.5 \cdot V_{fine} \quad (2.3)$$

$$= 1.5 \cdot V_{bg} - 0.5 \cdot (1637.79 \text{ mV} - N_{DAC} \cdot 3.1445 \text{ mV}) \quad (2.4)$$

can be calculated.

The eMUSIC board was designed at the University of Freiburg. A graphic of the board is shown in Figure 2.7. Its heart is the eMUSIC ASIC (U1). In order to program the ASIC, the ATmega328P-AU microchip (U4) is placed on the board. The microchip can be programmed with the Atmel Studio software by Atmel and the AVRSPi mkII porgrammer, which is connected to the computer via USB and can be plugged into the J4 connector on the eMUSIC board. After programming the microchip, it only has to be programmed again if the reset button SW1 is pressed.

Then the eMUSIC ASIC can be configured by using a TTL-to-USB adapter connected to a computer and the P3 connector, and the software of the minimusic board. The minimusic board is a commercial product using the eMUSIC ASIC. Due to the eMUSIC board being designed to work with the minimusic software, one avoids the need to write software and also has the security that the used software

was tested and is working correctly. Two functions of the minimusic software are not usable on the eMUSIC board, the calibration of the threshold and the calibration of the DC offset on the outputs. Therefore these two need to be set by the user.

The high voltage for the SiPMs can be supplied via the P2 SMA connector. On the backside of the PCB is an LSHM-150-060-F-DV-A-N-K connector located to connect the board to the SiPM board. Via this connector, the high voltage is brought to the SiPMs, and the signals are brought to the eMUSIC inputs. The eight single-ended outputs are applied to the SMA connectors K1 to K8. The fast OR signal can be read out via the K9 connector. Both the high and low gain differential summation outputs are connected to the pins of the J6 connector.

The board also provides the possibility to power upto six LEDs soldered onto the SiPM boards via the P1 connector. However, the usage of this is not advised since this will introduce interferences into the signals.

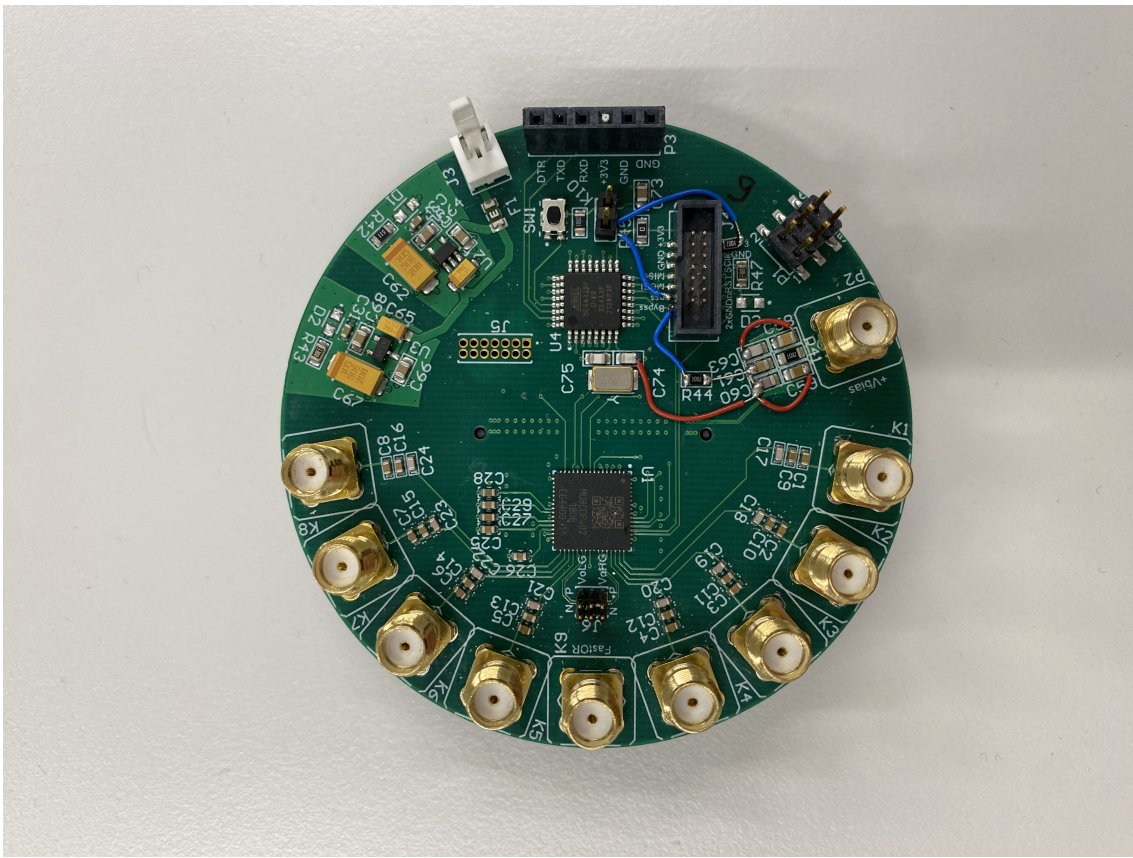


Figure 2.7: Picture of the eMUSIC board with the eMUSIC ASIC, the eight single-ended channel-by-channel SMA signal outputs, the SMA fast OR output, the differential signal output, the SMA connector for the high voltage supply of the SiPMs, and the connectors to program and power the board.

2.5 The GANDALF Module

The amplified and shaped output signal of the eMUSIC ASIC needs to be digitized for further analysis. For this step the GANDALF module could be employed. Originally developed at the University of Freiburg for the Common Muon Proton Apparatus for Structure and Spectroscopy (COMPASS) experiment, it has a modular design to fill different roles in the experiments Data Acquisition (DAQ). Using mezzanine cards, different signal, clock, and trigger inputs can be chosen. In the following, the GANDALF module will be shortly introduced. The mezzanine cards not used in this work are therefore only mentioned but not presented in detail. An overview of a GANDALF module is shown in Figure 2.8.

2.5.1 Input Mezzanine Cards

Each GANDALF module has two mezzanine card slots for input signals. In this thesis Analoge Mezzanine Cards (AMCs) with eight sampling Analog to Digital Converters (ADCs) were used.

The AMC is designed to digitize analog input signals. For digitization, eight ADC are used. There are AMC with two different ADC available. One is the *ADS5463*, with 12 bit and up to $500 \frac{\text{MS}}{\text{s}}$, and the other is the *ADS5474* which samples with up to $400 \frac{\text{MS}}{\text{s}}$ at 14 bit. The Effective Number of Bits (ENOB) of both ADCs are 10.4 bit and 11.2 bit, respectively. Each AMC has eight SMC connectors for the analog inputs. There are AMC operating in *normal mode*, meaning each SMC connector is connected to one ADC, resulting in eight channels with up to $500 \frac{\text{MS}}{\text{s}}$ or $400 \frac{\text{MS}}{\text{s}}$ per AMC. In order to increase the sampling frequency, AMCs which operate in the so called *interleaved mode* were built. On these AMCs, four inputs are connected to two ADCs each, and therefore every second SMC connector is a dead end. The clock signals which provide the sample tact for the two ADCs of one channel have 180° phase offset with respect to each other. By this, the sampling frequency is doubled to up to $1 \frac{\text{GS}}{\text{s}}$ or $800 \frac{\text{MS}}{\text{s}}$, at the cost of a reduced number of channels. The dynamic input range of the AMC is 4.4 V and can be shifted from the negative unipolar range -4.4 V to 0 V up to the bipolar range -2.2 V to 2.2 V . This shifting is done by an *AD5665R*, a 16 bit digital to analog converter. The dynamic range

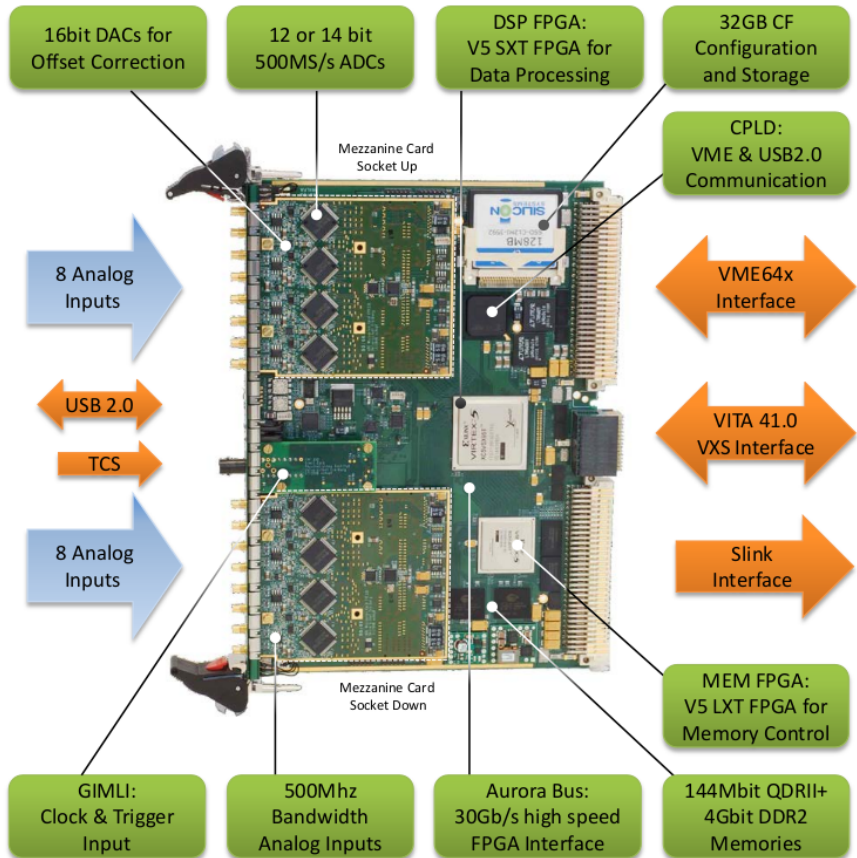


Figure 2.8: Overview of the GANDALF module equipped with Analog Mezzanine Cards (AMCs) and the fiber Gimli mezzanine card for clock and trigger input. The analog waveforms are digitized by the AMCs, and the digitized data is processed by the DSP FPGA. The MEM FPGA handles the memory of the processed data, which can be transferred to a computer via the USB interface on the front of the VME or S-Link interfaces on the backplane. [16]

was chosen because in the COMPASS experiment, for which the GANDALF was developed, negative voltage pulses created by Photomultiplier tubes (PMTs) needed to be digitized. However, because the used ADCs expect positive differential signals, inverting operational amplifiers are used to change the polarity of the signal. By changing the gain of the amplifiers, one can decrease the input range and therefore increase the amplitude resolution. The AMCs used in this thesis are 12 bit AMCs in the *interleaved mode* and a dynamic range of 2.2 V.

2.5.2 GIMLI Mezzanine Cards

A third mezzanine card slot is foreseen for the GIMLI mezzanine cards. These serve as clock and trigger interface. For this mezzanine card, three different options were developed. One GIMLI card, which takes the clock and trigger from the backplane, if one wants to use the create to distribute the signals. The fiber GIMLI has one fiber input to receive the clock and trigger via optical fiber. And the copper GIMLI, which was used for this work and is presented in the following.

The copper GIMLI, shown in Figure 2.9, provides the option to use an external or an internal clock. If only one GANDALF module is used, the internal 20 MHz clock of the copper GIMLI can be used. It is provided by an onboard oven-controlled oscillator (OCXO) with a jitter of less than 2.3 ps. In case two or more GANDALFs are used, an external clock is required to ensure a synchronized clock on all GANDALF modules. For this case, the copper GIMLI has a LEMO connector as input for an external clock with Nuclear Instrumentation Module (NIM) signal standard. Via a second LEMO connector, an external NIM trigger signal can be connected to the GANDALF module.

2.5.3 Usage of the GANDALF with SiPMs

In this work, the GANDALF was used for digitizing the output signal of the eMUSIC ASIC. As mentioned above in ??, these signals have a positive polarity. But because the GANDALF was designed for the digitization and processing of negative voltage pulses created by a PMT, this caused some problems. Since after the inverting operational amplifiers in the GANDALF, the SiPM signals have a negative polarity,



Figure 2.9: Picture of the copper GIMLI with an internal 20 MHz clock generated by an onboard oven-controlled oscillator. With the LEMO connectors external clock and trigger NIM signals can be provided for the GANDALF. [16]

the input voltage range needs to be chosen to be bipolar and around -1.1 V to 1.1 V . Also, the self-trigger of the GANDALF needed to be adjusted. It functions via samples over threshold. The user can set a threshold and a number of consecutive samples which need to be over the threshold for the GANDALF to trigger an event. Since after the inverting of the positive signals, the signals have a negative polarity, and the threshold needs to be set to a lower ADC value than the baseline. In addition to that, the sample over threshold condition in the GANDALF firmware needed to be inverted to trigger if a number of consecutive samples were below the threshold. The new firmware with the inverted trigger condition was tested and worked as intended, with the exception of one bug. If the data rate from the GANDALF to the DAQ computer exceeds the maximum possible data rate, $20 \frac{\text{MB}}{\text{s}}$ in the case of the USB interface, incomplete events will be written down to disk. This is most likely caused by a missing VHDL file that was not included in the new firmware and which would, in case the buffer of the GANDALF is completely filled, prevent the GANDALF from sending incomplete events to the computer. For the intended use of this bug should not be a problem since the data rate is expected to be way below the possible $20 \frac{\text{MB}}{\text{s}}$.

Chapter 3

Setup

In this chapter, the setup with which the different tests with the eMUSIC boards were performed is described. First the SiPMs and the SiPM boards are shown, then the dark box, in which the SiPM boards were placed for the tests. Lastly the setup part with the GANDALFs is described.

3.1 SiPM

An important part of the setup are of course the SiPMs which generate the charge signal which then gets amplified by the eMUSIC chips. The SiPMs mainly used in this work are the *S14160-3050HS* by the manufacturer Hamamatsu. During the Deutsches Electronen SYnchrotron (DESY) testbeam also the SensL *J-Series 30035* manufactured by Onsemi were used besides the *S14160-3050HS*. A few important parameters of both SiPM models are listed in Table 3.1. The SiPM boards which were used in this work have forty SiPMs soldered onto them. These boards exist with both SiPM models. A picture of the front and back side of a Hamamatsu SiPM board is shown in Figure 3.1. A breakout board can be plugged in on the back of the PCB. For this thesis the eMUSIC board, which is described in the previous chapter, was plugged onto the SiPM board.

Table 3.1: Relevant parameters of the both used SiPM models by Hamamatsu and Onsemi. [17, 18]

parameter	S14160-3050HS	SensL
photosensitive area / mm ²	3.0×3.0	3.07×3.07
pixel pitch / μm	50	35
number of pixels	3000	5676
spectral response range / nm	270 to 900	200 to 900
peak sensitivity wavelength / nm	450	420
breakdown voltage / V	38	24.2 to 24.7
recommended operating voltage / V	40.7	25.2 to 30.7
variation of rec. op. voltage (typ. / max) / V	0.1 / 0.2	
gain	$2.5 \cdot 10^6$	

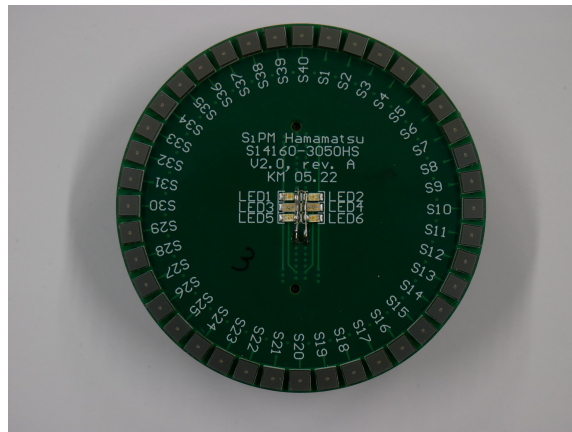


Figure 3.1: One of the PCBs with Hamamatsu SiPMs used for this work.

3.2 Dark Box Setup

To ensure a controlled environment with controlled light exposure of the SiPMs for the measurements, the SiPMs were placed inside a dark box. The inside of the box is covered in black aluminum foil made by Thorlabs with a reflectivity in the visible wavelength spectrum below 5 % [19]. An optical rail for fixing the SiPM board, a diffusor and the end of an optical fiber was placed in the box. Via the optical fiber the light of a 460 nm LED can be guided into the box. The LED is inside of another light tight box. It was build as part of the bachelor thesis of Alexander Bismark and is described there in more detail [20]. Power can be supplied to the LED via a BNC connector on the light tight box. In this thesis the Tektronix AFG was used to create voltage pulses with a width of 4 ns with 2.5 ns rising and falling edges. To illuminate all SiPMs equally a *ED1-C50-MD* diffuser by Thorlabs was used. A light beam hitting the diffusor perpendicular to its surface gets diffused in a circular shape with a 50° opening angle.

Multiple BNC, SMA, and SMC feedthroughs were installed in the dark box to supply the SiPMs and eMUSIC board with power and to transfer the output signals of the eMUSIC out of the box to a digitizer or oscilloscope. Also a hole drilled to insert the optical fiber from the LED setup into the box and afterwards covered, to block light from entering through the hole. A power supply was used for the high voltage supply of the SiPMs. If not otherwise specified, all measurements shown in this thesis were done with a high voltage of 43 V. To control the voltage the HP multimeter was used instead of the less precise voltage display of the power supply. The eMUSIC board was powered by a 8 V power supply. For the digitization either a GANDALF or the Tektronix oscilloscope was used.

Figure 3.2 shows a schematic sketch of the setup inside and on the outside of the box. A picture of the setup inside the box is shown in Figure 3.3. It includes the LED fiber, the diffuser, the SiPM and eMUSIC board with power and signal cables attached. In the following the setup part with the GANDALF is described.

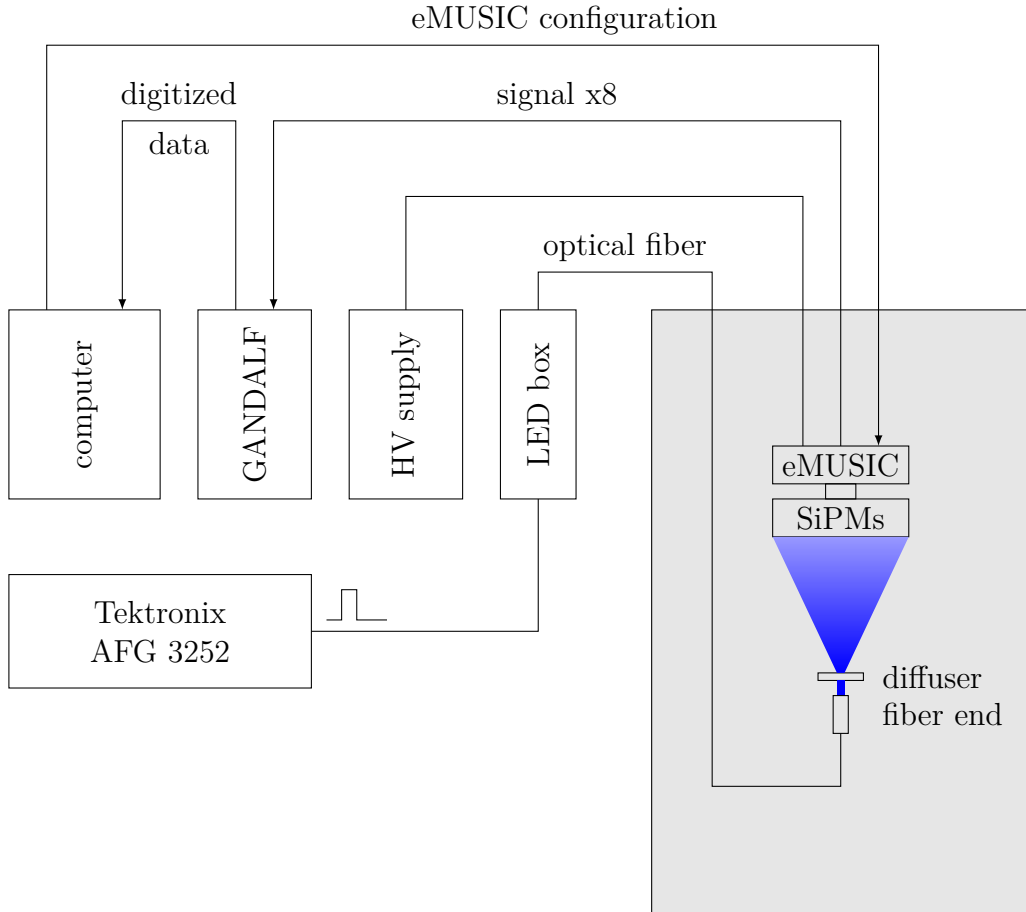


Figure 3.2: Schematic view of the measurement setup. The eMUSIC board and SiPM board are in a dark box to prevent unwanted light exposure. The high voltage for the SiPMs is supplied by a power supply outside the box. An 8V power supply provides the power for the eMUSIC board. A computer is used to configer the eMUSIC chip. The output signals of the eMUSIC board are digitized by aGANDALF and then send to the computer, where they are written to disk. With voltage pulses from an arbitrary function generator a LED is powered. The emitted light is guided into the dark box through an optical fiber. In the box the fiber is mounted in front of the SiPMs with a diffuser between the fiber end and the SiPMs.

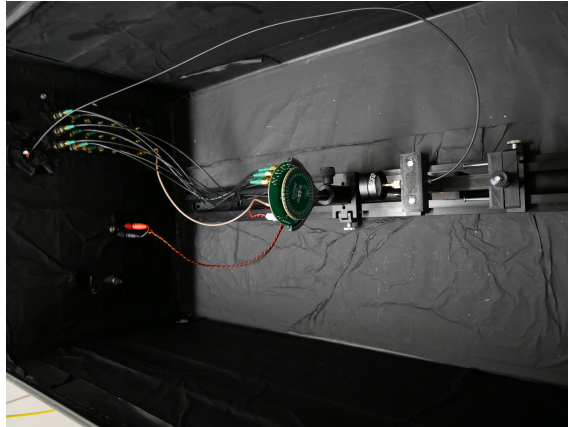


Figure 3.3: The inside of the dark box which was used for the test measurements. On the left is the end of the fiber from the LED setup mounted on the optical rail. Behind the fiber end is a diffuser by Thorlabs which diffuses the light in a circular distribution with an opening angle of 50° . After the diffuser is the PCB with the SiPMs placed. On its back is the eMUSIC board plugged in. The high voltage for the SiPMs is supplied via the brownish cable, the power for the eMUSIC chip is supplied with the red and black cable and the signal outputs of the eMUSIC boards are connected with the feedthrough on the box via the black SMA cables.

3.3 Gandalf

For the operation of the One Cell Prototype sixteen channels need to be digitized, eight of each of the two WOMs. Therefore two GANDALFs are required. In order to save place and simplify the setup, the GANDALFs are not operated in a VME crate but are each in a GANDALF portable. It is a mobile case made exactly for such purposes where a whole crate is unconvienient to use. A picture of a GANDALF portable is shown in ???. Due to the usage of two GANDALFs an external clock is required to ensure a syncronized sampling frequency and clock for time stamps. As an external clock a copper GIMLI was chosen and used with a GIMLI testboard, shown in ???. It has two slots for GMILIs with a clock output for each slot and a power connector to supply it with 5 V. For the purpose of an external clock, only one of these slots and the corresponding clock output is used. Via LEMO cables, the clock signal form the boards clock output pins is connected to the clock inputs of the GANDALFs.

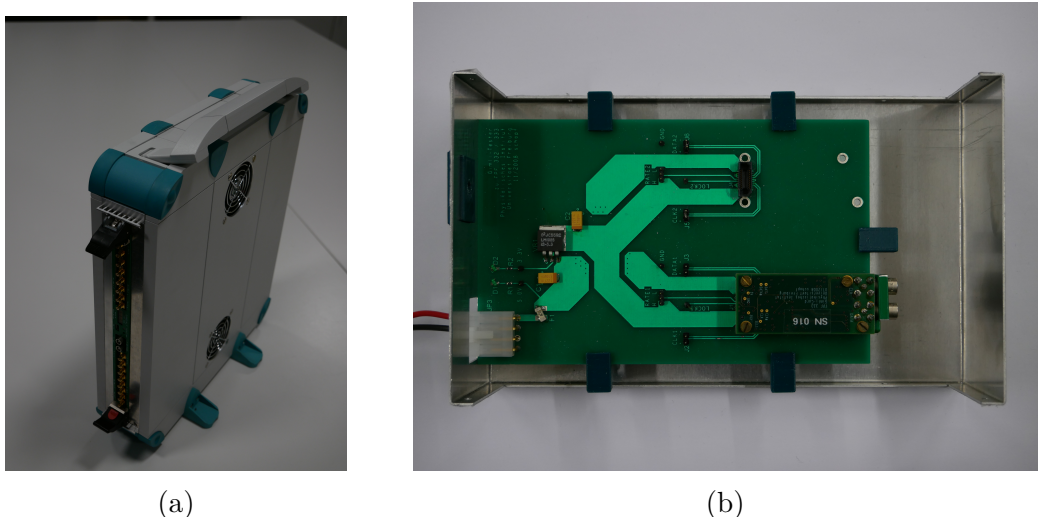


Figure 3.4: A GANDALF portable equipped with a GANDALF. The GIMLI test board with a copper GIMLI

Chapter 4

Results of the DAQ Tests

4.1 GANDALF Clock Frequency and ADC Test

Before using the GANDALF modules in the DAQ, they need to be checked for proper functioning. For this, two things are relevant: One is the quality of the sampling clock, the other the differential linearity and monotonyty of the ADCs. To perform these tests, a 150 MHz sine voltage signal was generated with an AWG and a narrow bandwith 150 MHz filter with a 3 dB bandwidth of ± 5 MHz [16]. The filter ensures a pure sine wave and unwanted frequencies are suppressed. The clean sine signal was then connected to the inputs of the GANDALFs, one after another. For each input 1000 waveforms were recorded, each with 430 samples. For each channel a Fast Fourier Transform (FFT) was done for one waveform using the python3 functions `scipy.fft.rfft` and `scipy.fft.rfftfreq` to find the sampled frequencies in the signal. ?? shows the plot with the FFT for channel 0 of the AMC 46 used with the GANDALF 23. In the plot the red line marks the center frequency of the measured signal. The measured peak frequency is determined by the maxima in the frequency spectrum and the uncertainty is estimated to be halfe the frequency steps of the FFT. The result of the FFT is a measured center frequency of (149.4 ± 1.0) MHz. Therefore the sampling frequency of the GANDALF is as intended, which means that the external clock signal is working correctly.

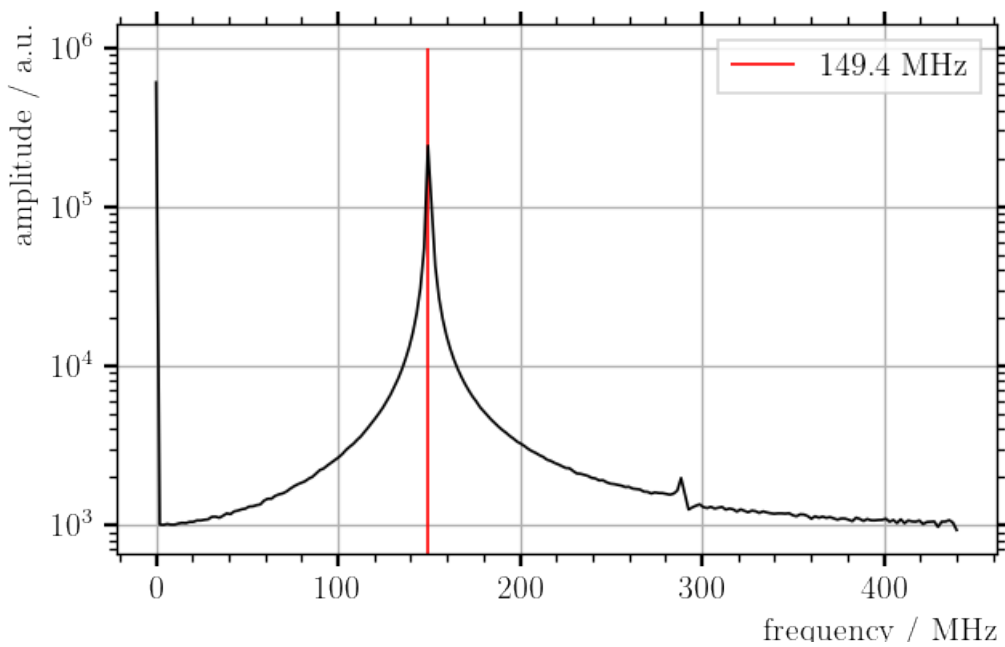


Figure 4.1: The FFT of a 150 MHz sin signal recorded with the GANDALF module 23 with a 880 MHz sampleing rate. The peak frequency is masured to (149.4 ± 1.0) MHz

4.2 Input Offset Voltage

The first measurement with the eMUSIC board is to find out the input offset voltage of the eMUSIC for different DAC values. This needs to be done to determine the correct overvoltage of the SiPMs, which influences among other things the gain of the SiPMs. In order to perform this measurement, the setup in ?? was assembled. The measurements were done for both the eMUSIC boards 2 and 6. The SiPMs were supplied with a high voltage of 4.7 V for a reverse bias voltage, as in normal operation. To prevent damages to the SiPMs, the high voltage was not increased over the breakdown voltage. For this measurement the eMUSICs input DAC settings, which can range from 0 to 511 DACu, were set to 0 DACu. Then the voltages between the negative high voltage pole and the voltage on the cathode of the SiPMs were measured. As measurement point for the cathode voltage, the 0Ω resistor placed on the back of the SiPM board was chosen. It is shown in ???. This measurement was done for one SiPM of each SiPM group. The chosen SiPM were 1, 6, 11, 16, 21, 26, 31 and 36. After measuring the different voltages, the DAC setting was increased in steps of 50 DACu up to 500 DACu and at each step the measurement was repeated. In the following first the measurement results of the individual channels over all tested DAC settings are presented. Afterwards, the input offset voltages of the different channels for the same setting are compared.

As an example, the measurements of all eleven tested DAC settings done with the eMUSIC board 2 and channel 0 are shown in Figure 4.2. In the upper part of the plot, the measured voltages are plotted and for the measurements with a DAC setting between 100 DACu and 450 DACu a linear fit was performed. The first two measured voltages were not included, since they visibly do not follow the linear trend. For all channels the first two measured values are at around 1530 mV which indicates a constant offset voltage below 100 ADCu. Depending on the eMUSIC board and the channel also the last measured voltages were excluded from the fit since they do not follow strictly the linear trend and increase on some eMUSIC channels to 940 mV. The resulting slope and offset of the linear fit are

$$V_{\text{offset, fit}} = (-3.438 \pm 0.028) \frac{\text{mV}}{\text{DACu}} \cdot x + (1830 \pm 8) \text{ mV} \quad \text{for } 100 \text{ DACu} \leq x \leq 450 \text{ DACu} \quad (4.1)$$

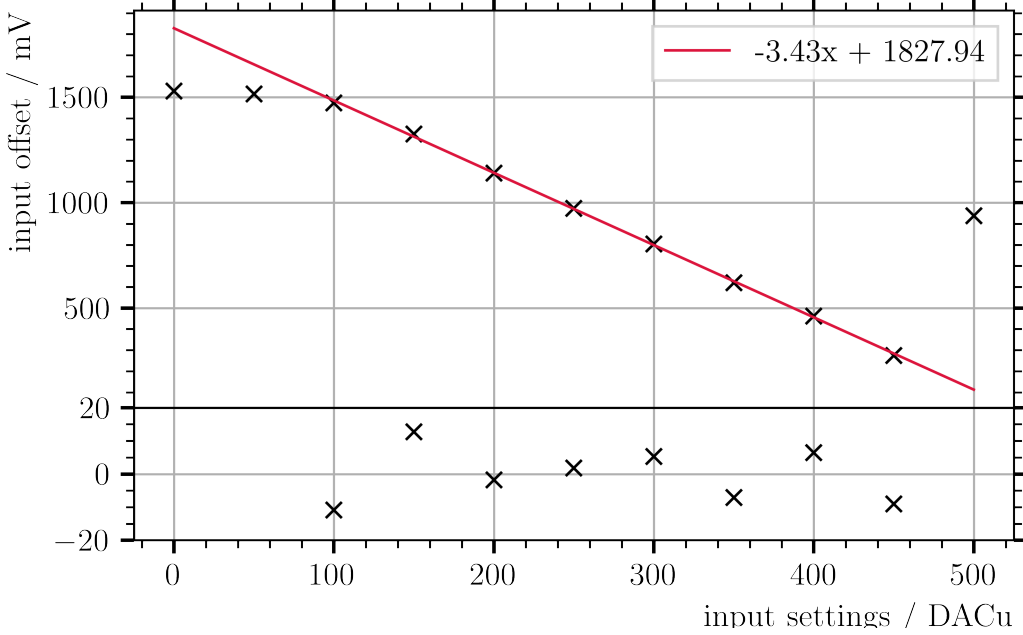


Figure 4.2: Input offset measurement for the channel 0 of the eMUSIC board 2. The input voltage was measured for input DAC settings from 0 DACu to 500 DACu in 50 DACu steps. A linear fit was performed for the measurements with DAC settings between 100 DACu and 450 DACu. The other measured voltages were excluded from the fit since they do not follow the linear trend. Below is the residual plot with a fixed y-axis window from -20 mV to 20 mV .

where x is the setting of the DAC in DACu. The bottom of the plot shows the residual plot where the difference between the linear fit and the measured values is shown. The range on the input-offset-axis is fixed to -20 mV to 20 mV . In Table 4.1 the fit results for the measurements with the eMUSIC boards 2 and 6 are listed. The DAC voltages of the channels differ to other channels on the same board as well as to the channels on the other board. Therefore the measurement of the input voltage should be done for every eMUSIC board.

To compare the differences between channels with the same DAC settings, for three different settings the input voltage was plotted for all eight channels in Figure 4.3. For settings at 50 DACu and below, the input offset voltage is pretty equal between the channels and only differs in the single mV range around 0 mV . A similar behavior is seen for DAC settings at and above 500 DACu, for which the input voltage is

Table 4.1: The result of fitting a linear function to the input offset measurements of the eMUSIC boards 2 and 6.

eMUSIC board	channel	slope / $\frac{\text{mV}}{\text{DACu}}$	offset / mV
2	0	-3.438 ± 0.028	1830 ± 8
	1	-3.405 ± 0.015	1818 ± 5
	2	-3.377 ± 0.016	1803 ± 5
	3	-3.336 ± 0.017	1778 ± 5
	4	-3.290 ± 0.018	1764 ± 5
	5	-3.316 ± 0.020	1758 ± 6
	6	-3.211 ± 0.019	1716 ± 6
	7	-3.163 ± 0.016	1702 ± 5
mean of all channels		-3.317 ± 0.011	1771 ± 3
6	0	-3.472 ± 0.019	1843 ± 5
	1	-3.353 ± 0.029	1804 ± 9
	2	-3.368 ± 0.028	1795 ± 8
	3	-3.389 ± 0.030	1801 ± 9
	4	-3.260 ± 0.050	1747 ± 12
	5	-3.202 ± 0.033	1729 ± 10
	6	-3.275 ± 0.015	1756 ± 4
	7	-3.263 ± 0.024	1749 ± 7
mean of all channels		-3.317 ± 0.013	1777 ± 4

around 940 mV and the differences between the channels is also in the single milliV range. But in the DACu range where the linear progression can be seen, the variations between the channels is larged, in some cases over 70 mV. This confirms, that calibration measurements of the input voltage needs to be done for all eMUSIC boards and all channels.

After these measurements were done, for the eMUSIC boards 2 and 6 the settings for which all channels have 1 V offset were determined. The resulting DAC settings and the corresponding input voltages are listed in Table 4.2. With these settings the measurement of the pole-zero cancellation and the low and high trans-impedance and pole-zero attenuation were performed. Which are presented in the following sections.

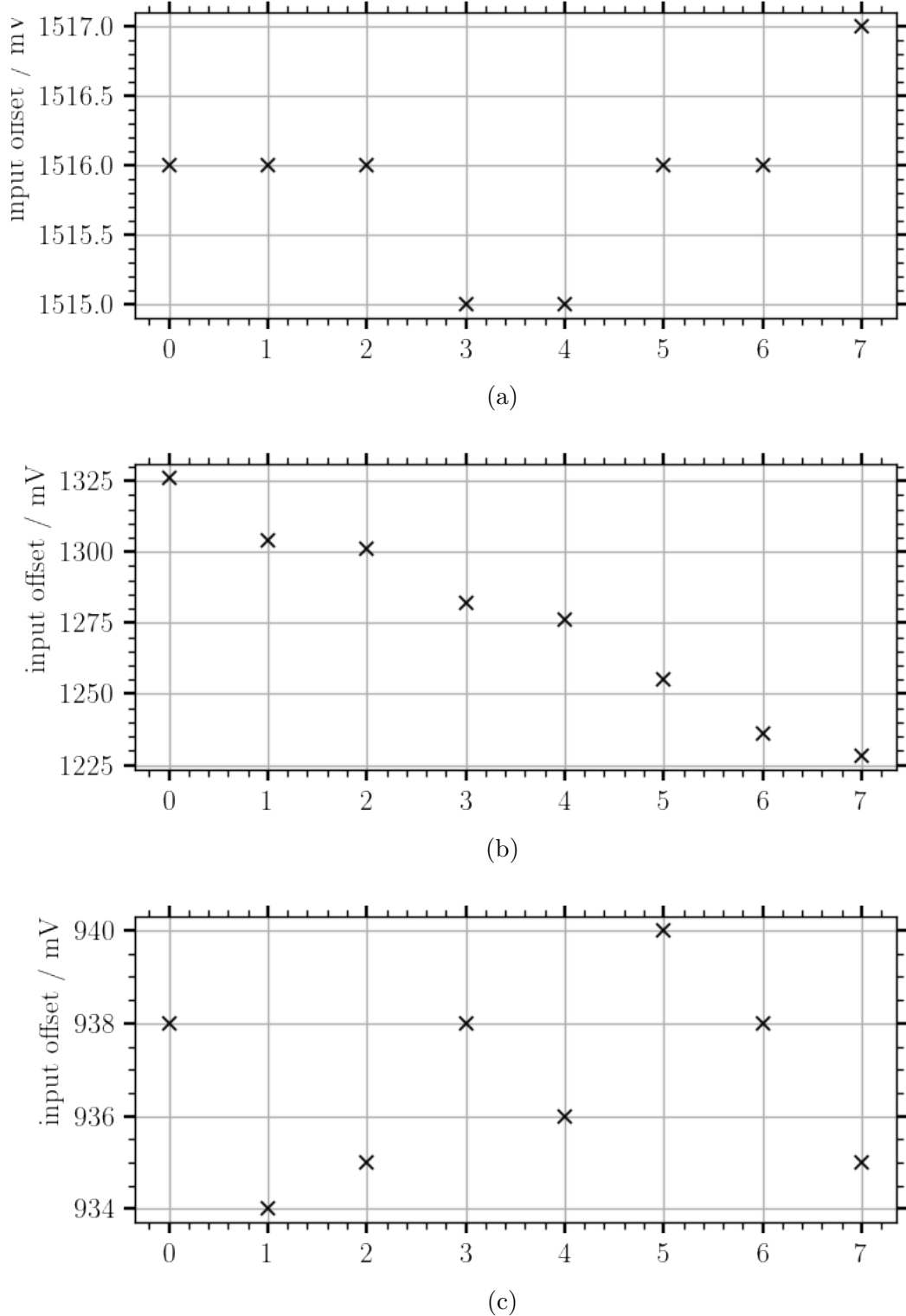


Figure 4.3: The input offset voltages of the different channels for the input DAC settings 50 a), 150 b), and 500 c). The shown measurements were done with the eMUSIC board 2. While the differences between the channels for the setting 50 and 500 are less than 10 mV, the maximum difference measured with the setting 150 is around 100 mV.

Table 4.2: The DAC settings for the eMUSIC boards 2 and 6 with which the input offset voltage is as near to 1 V as possible. The uncertainties of the measured voltages is estimated from the fluctuations during the measurement to be 1 mV.

eMUSIC board	channel	DAC setting / DACu	input offset / mV
2	0	0	1003
	1	50	1001
	2	100	1003
	3	150	1004
	4	200	1003
	5	250	1002
	6	300	1002
	7	350	1002
6	0	0	999
	1	50	998
	2	100	997
	3	150	1003
	4	200	1002
	5	250	995
	6	300	996
	7	350	1001

4.3 Pole-Zero Cancellation Shaper

In this section the results from the characterization of the pole-zero cancellation shaper and its effect with different settings are described. Hereby the amplitude of the peak and the FWHM are of interest. The tests were done using the setup described in ???. The high voltage for this and all following measurements, as long as not otherwise stated, was set to 43 V. A GANDALF module was used for the digitization. The eMUSIC settings of one of these measurements are shown in Figure 3.4 in the appendix. For the other measurements, only the pole-zero settings were changed. Each measurement includes approximately 80 000 events, for which the mean waveforms are shown in the plots below. The values for the amplitude and FWHM were calculated for each individual waveform and their mean values are presented here for the different measurements.

First the pole-zero cancellation was disabled to perform measurements for a reference amplitude and FWHM. In Figure 4.4 the mean of all 80 000 waveforms is shown. The mean amplitude is

$$V_{amp} = (523 \pm 46) \text{ mV} \quad (4.2)$$

and the FWHM is

$$t_{FWHM} = (113 \pm 3) \text{ ns.} \quad (4.3)$$

Next the measurement with enabled pole-zero cancellation and with fixed settings for its capacitor and varying resistor values. The resistor settings were changed to all possible values, from 0 to 7, and the capacitor setting was kept at 31. Figure 4.5 presents the mean waveforms for the eight measurements. The determined amplitudes and FWHM and the corresponding decrease in respect to the values without pole-zero cancellation are listed in Table 4.3. For higher resistor values, the amplitude decreases from $(354 \pm 30) \text{ mV}$ for the setting 0 down to $(143 \pm 13) \text{ mV}$ for the setting 7. Also the FWHM decreases down to $(10.2 \pm 0.6) \text{ ns}$ with higher resistor settings.

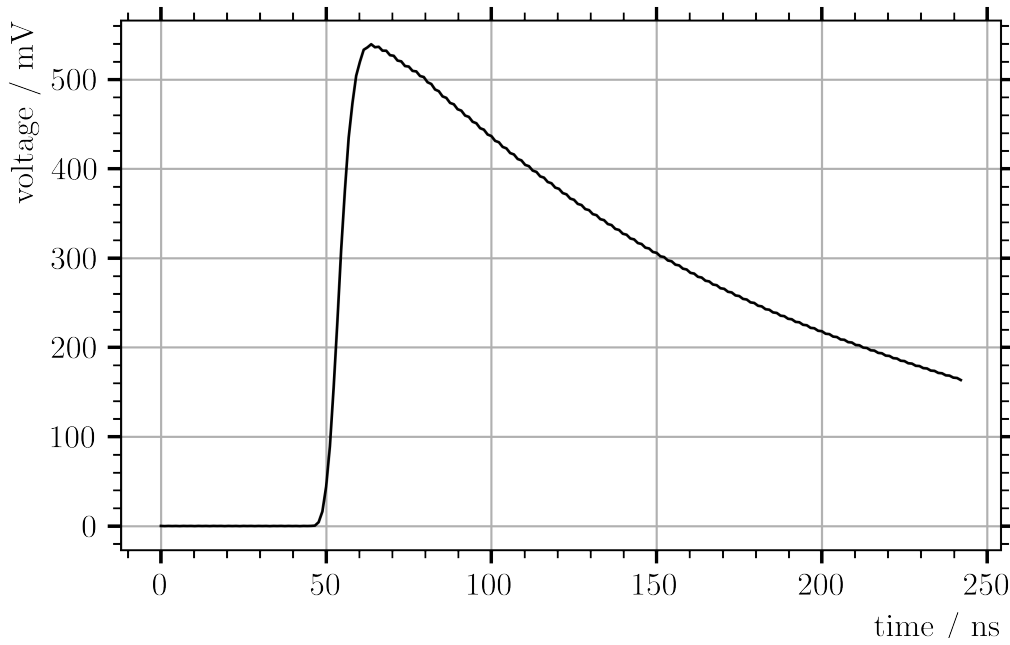


Figure 4.4: Mean waveform for a measurement without pole-zero cancellation.

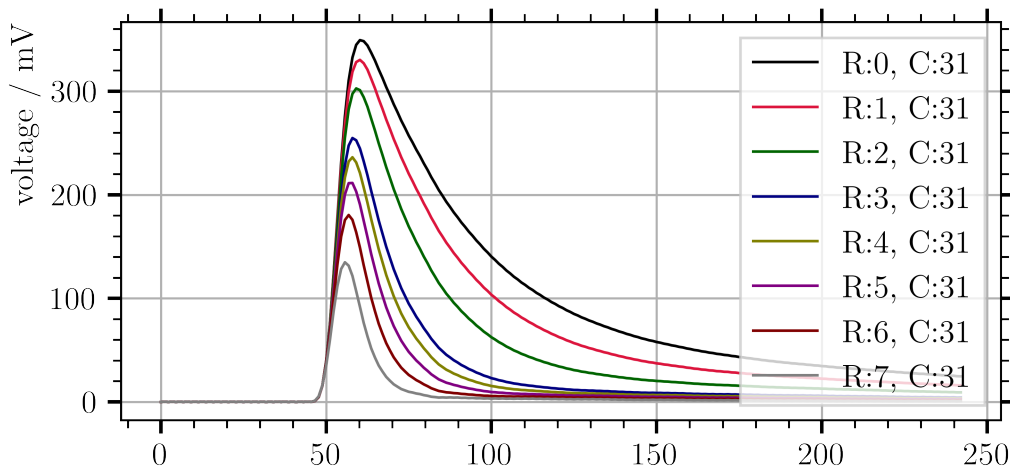


Figure 4.5: Mean waveform for different pz-cancellation resistor values. The pole-zero cancellation capacitor setting was kept at 31. With increasing resistor settings the amplitude decreases and the width of the peak becomes smaller.

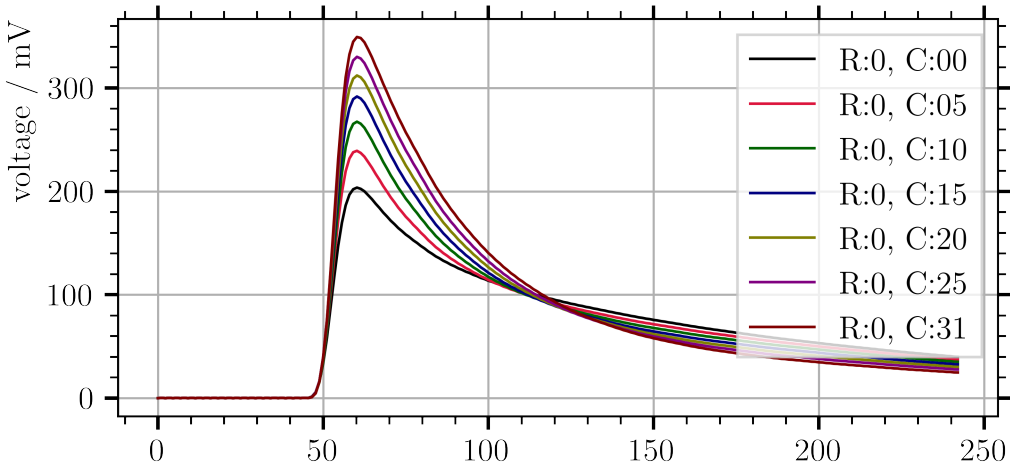


Figure 4.6: Mean waveform for different pz-cancellation capacitor values. The resistor settings were kept at 0 for all of the seven measurements.

The measurements with different capacitor settings were performed with the resistor setting of 0. For the different measurements, the capacitor settings were changed to all 32 possible values, from 0 to 31. In Table 4.3 the mean values for the maximum amplitude and the FWHM as well as the decrease compared to the values with disabled pole-zero cancellation are listed. The mean waveforms for the measurements with the capacitor settings 0, 5, 10, 15, 20, 25, and 31 are shown in Figure 4.6. Similar to the effect of the resistor, with higher capacitor settings, the FWHM decreases. For the setting 0 it is and with the maximal setting 31 it is decreased to (36.8 ± 1.1) ns. But, opposite to the resistor setting effects, the signal amplitude increases with higher settings up to (354 ± 30) mV. The minimal amplitude value, with the capacitor setting 0, is (206 ± 17) mV. So by adjusting the capacitor, the amplitude can be increased by a factor of 1.7 ± 0.3 .

Table 4.3: The amplitudes and FWHMs measured with different resistor and capacitor settings for the pole-zero cancellation. For each setting, around 80 000 waveforms were recorded. The listed values are the mean amplitudes and FWHMs of all corresponding waveforms.

R	C	amplitude / mV	FWHM / ns
-	-	523 ± 46	113 ± 3
0	31	354 ± 30	36.8 ± 1.1
1	31	335 ± 29	30.5 ± 0.9
2	31	308 ± 27	24.4 ± 0.8
3	31	262 ± 23	17.5 ± 0.6
4	31	243 ± 21	15.7 ± 0.6
5	31	220 ± 19	14.0 ± 0.6
6	31	188 ± 17	12.1 ± 0.5
7	31	143 ± 13	10.2 ± 0.6
0	0	206 ± 17	58.1 ± 2.7
0	5	242 ± 21	43.2 ± 1.7
0	10	271 ± 23	38.7 ± 1.4
0	15	296 ± 25	36.9 ± 1.2
0	20	316 ± 27	36.5 ± 1.2
0	25	334 ± 28	36.4 ± 1.1
0	31	354 ± 30	36.8 ± 1.1

4.4 Transimpedance and Pole-Zero Attenuation

After investigating the effects of the pole-zero shaper the influences between the normal and the low pole-zero attenuation settings are examined. Also the high and low transimpedance settings are investigated.

First the pole-zero attenuation was looked at. Therefore another measurement without the lower attenuation setting was performed. The pole-zero cancellation resistor setting was set to R=3 and the capacitor setting was set to C=31. In Figure 4.7a the mean waveforms with and without lower attenuation are presented. The peak of the waveform is not affected by the lower attenuation setting. Mainly the tail is of the waveform is increased in amplitude by using the lower attenuation. This increases the peak width, but as it can be seen in Figure 4.7a it can also prevent small overshoot of the signal.

The measurement was also done with the pole-zero settings 7 and 0 for the resistor and capacitor, respectively. The result is shown in Figure 4.7b. Here the same behavior can be observed. The peak amplitude is not influenced, only the amplitude of the tail is increased by the lower attenuation.

Next, the high and low transimpedance settings were investigated. Therefore two measurements without pole-zero cancellation were taken, one with high and a second with low transimpedance. Again, both measurements consist of around 80000 waveforms. Mean waveforms were calculated for both measurements and plotted in Figure 4.8. The mean amplitude of the events with high transimpedance is

$$V_{\text{high imp}} = (540 \pm 50) \text{ mV} \quad (4.4)$$

and of the events with low transimpedance the mean amplitude is

$$V_{\text{low imp}} = (185 \pm 14) \text{ mV}. \quad (4.5)$$

This results in a reduction by the factor 0.34 ± 0.04 if the low transimpedance is used. The measurements were repeated with the settings 3 and 31 for the pole-zero resistor and capacitor, respectively. The mean amplitudes for these measurements

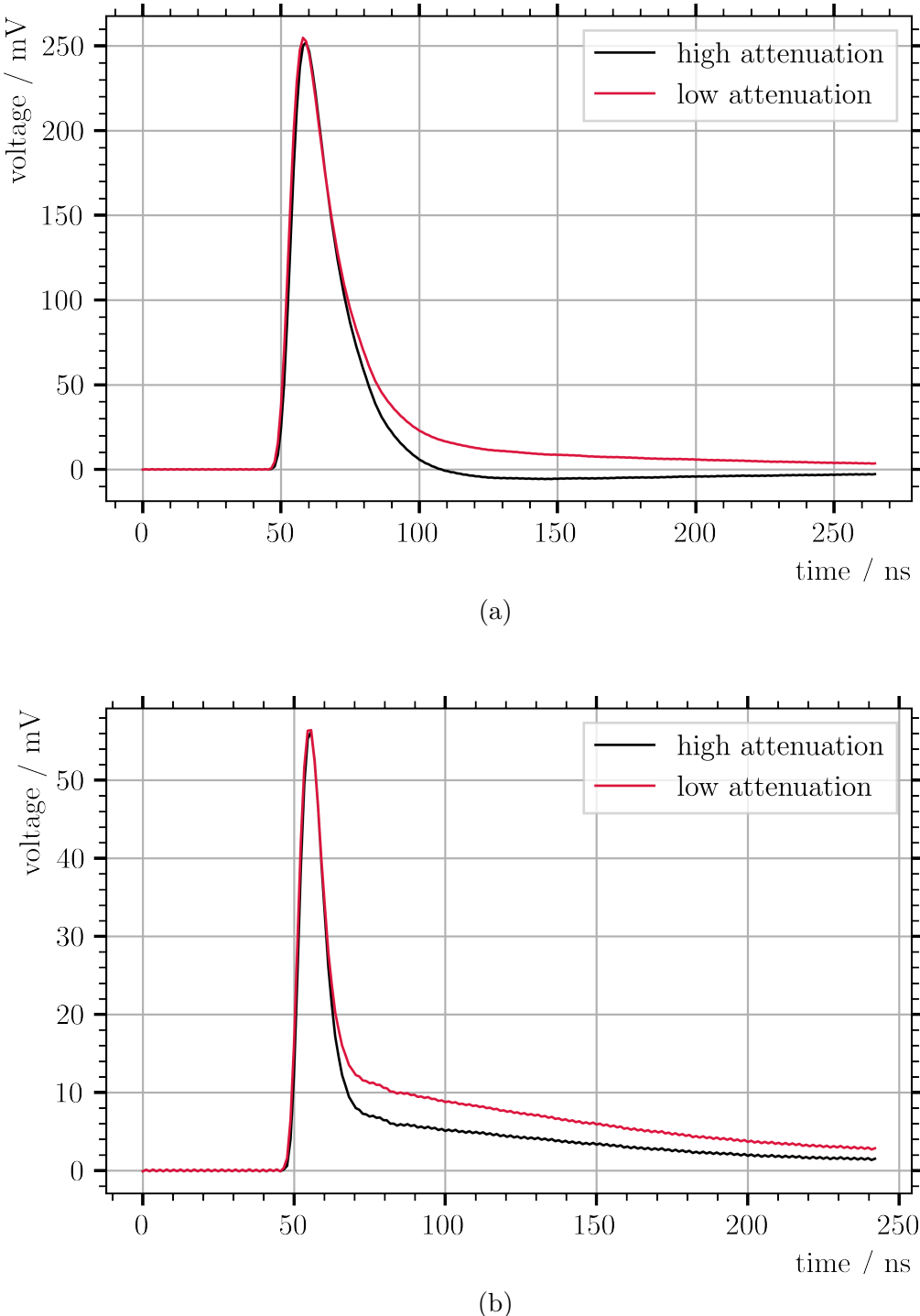


Figure 4.7: The mean waveforms of two measurements, each around 80 000 waveforms, with the pole-zero settings 7, for the resistor, and 00 for the capacitor. One measurement was done with the low attenuation option of the eMUSIC and the other was done without that option. Mostly the tail of the peaks is affected by the low attenuation option, while the peak amplitude seems to be not changed.

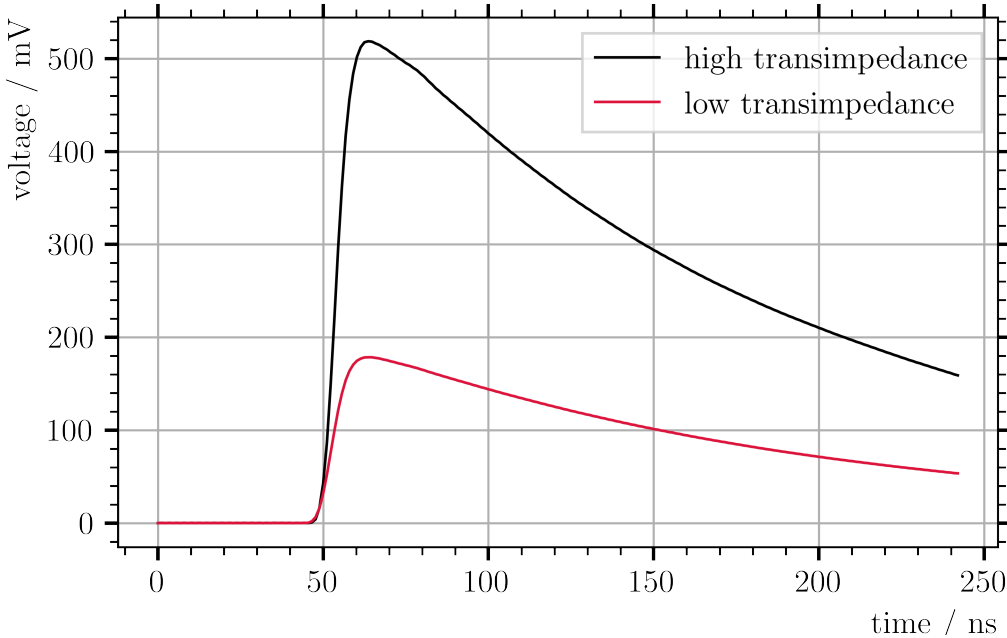


Figure 4.8: The mean waveforms of two measurements with around 80 000 waveforms each. The black waveform corresponds to a measurement done with high transimpedance and the red waveform corresponds to a measurement with low transimpedance.

are

$$V_{\text{high imp}} = (272 \pm 22) \text{ mV} \quad (4.6)$$

$$\text{and } V_{\text{low imp}} = (94 \pm 7) \text{ mV} \quad (4.7)$$

and the factor by which the signal amplitude decreases is 0.35 ± 0.04 , which is also in agreement with the results of the other measurement. The plots of the mean waveforms for the measurements with pole-zero cancellation are shown in the appendix in Figure 3.4.

4.5 Dark Count Measurements

The measurement of dark counts can be an easy way to calibrate the gain of the readout. To test if this is possible with the eMUSIC as amplifier, two dark count measurements were performed. For the first measurement, to maximize the amplitude, the pole-zero calibration was disabled and the high transimpedance setting was used. The second dark count measurement was done with enabled pole-zero calibration, low attenuation and high transimpedance. For the resistor and capacitor of the pole-zero cancellation the settings 3 and 31 were chosen, respectively. Since the amplitude of dark counts is in the lower mV range and therefore not much higher than the electronic noise, a measurement of the noise with a high voltage of 20 V was performed for comparison. To maximize the amplitude resolution, the oscilloscope was used instead of a GANDALF module. In Figure 4.9 the histograms with the integrals of a 136 ns time window around the trigger point is shown. The comparison of the dark count measurements with the noise measurement shows, that dark counts were measured. But it no single photoelectron peaks can be distinguished with the measurement with pole-zero cancellation. Hence, the calibration using dark count measurements is not possible in that case. The histogram with the dark count measurement result without pole-zero cancellation is shown in Figure 4.10 Also here no single photoelectron peaks can be distinguished. Hence also without the pole-zero cancellation no calibration is possible.

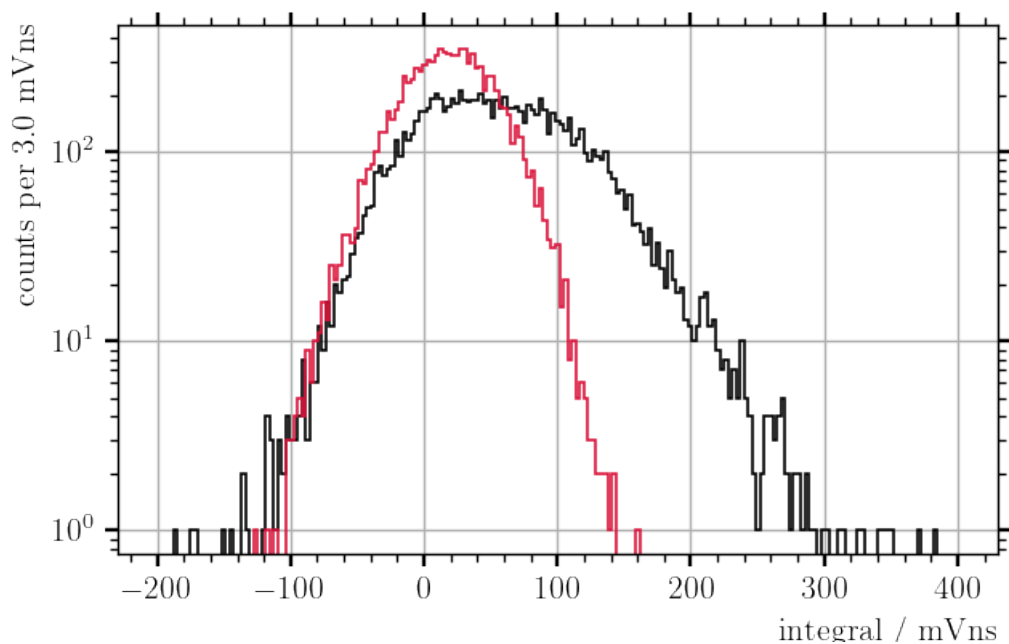


Figure 4.9: The histogram of the dark count measurements with pole-zero cancellation, and the electric noise measurement. No single photoelectron peaks can be distinguished in the dark count measurement histograms. Therefore dark count measurements cannot be used for calibration.

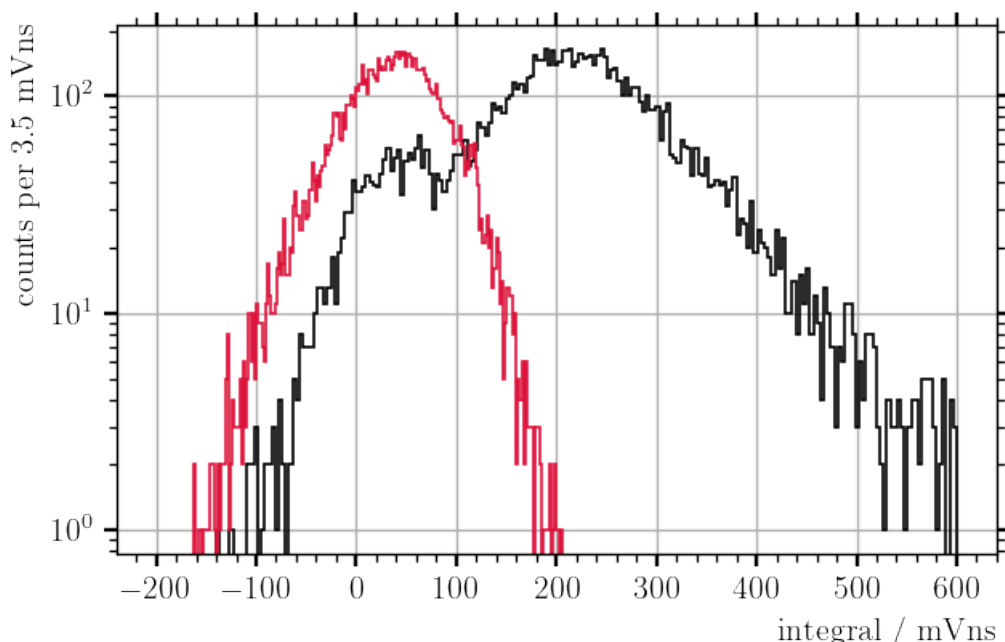


Figure 4.10: The histogram of the dark count measurements without pole-zero cancellation, and the electric noise measurement. No single photoelectron peaks can be distinguished in the dark count measurement histograms. Therefore dark count measurements cannot be used for calibration.

Chapter 5

DAQ Performance at the DESY Testbeam

In october 2022 the One Cell Prototype was tested for one week at the DESY testbeam. Figure 5.1 shows a picture of the the One Cell Prototype set up at the testbeam area. The electron beam comes from the right, where it first passed a $2 \times 2\text{ mm}^2$ square lead collimator. Afterwards the electrons passed four plastic scintillators which are read out with PMTs. A coincidence of the signals from all four PMTs is used to trigger the data aquisition. After the scintillators the One Cell Prototype is placed. It stands on a rotary table to allow measurements with the beam coming from different angles, and on a DESY table, which enables left-right and up-down movement. Measurements of each 10000 events were performed for XX positions by adjusting the position of the DESY table. Each position was measured at different angles from 0° to 90° in 15° steps by turning the detector on its rotary table. For all positions and angles five measurements were done with variing beam energy starting from 1.4 MeV up to 5.4 MeV in 1 MeV steps.

During the testbeam the WOMs were read out with Hamamatsu SiPMs, except for a few measurements using the SensL SiPMs for comparisson. The optical coupling between the WOMs and the SiPMs was done with silicon pads. Test measurements were performed using optical gel instead of the silicon pad, since the optical gel was used in previous testbeams. The SiPM signals were amplified and shaped by eMUSIC ASICs with eMUSIC boards. The eMUSIC configuration used for most

Figure 5.1: Picture of the One Cell Prototype set up in the DESY testbeam area. The electron beam is coming from the right and is focused by a lead collimator. After the collimator the beam telescope consisting of four plastic scintillators and PMT is placed as a trigger for the data aquisition. Next to the beam telescope is the One Cell Prototype. It is placed on a rotatory table and a DESY table for left-right and up-down movement. The power supplies and the digitizer are not shown in this picture.

of the measurements is shown in the appendix. A few measurements used the settings but without the high transimpedance. The low transimpedance was chosen espacially for a measurement where the electron beam was shot directly through the lower WOM since the output of the eMUSIC saturated with the high transimpedance setting. The digitization was done by a 64 channel WaveCatcher. It is a 12 bit digitizer with a sampling frequency of up to $3.2 \frac{\text{GS}}{\text{s}}$ and a dynamic range of $2.5 \text{ V}_{\text{pp}}$. The WaveCatcher also digitized the signals from the four beam telescope PMTs and triggered on a coincidence with a threshold of 17 mV . To supply the eMUSIC board with power, the same power supply used for the test measurements shown in the previous chapter is used. For the power of the SiPMs a custom, remote controllable power supply was build by Tim Molzberger in Freiburg.

After the performance of the DAQ was tested at the testbeam for one week with particles of known energy and known direction of movement, the long term performance of the one cell prototype and the DAQ needs to be investigated. For this purpose, the one cell prototype is assembled at the University of Freiburg, where it is supposed to be taking continuously data for a year. Here the majority of events will be caused by cosmic muons. By adding plastic scintillators with PMTs above and below the detector, trigger the data aquisition on a coincidence to only measure events, where the particle passed vertically through the detector. Also a way to calibrate the detector needs to be found.

Chapter 6

Summary and Outlook

In this thesis a DAQ for the readout of WOMs was assembled and tested. It consists of eMUSIC boards with eMUSIC chips for signal amplification and shaping and GANDALF moduls for digitization. In the future it is supposed to be used for the long term test of the so called “One Cell Prototype” in Freiburg.

A external clock was prepared for the GANDALFs and tested for proper functionality. This test was done by generating a pure 150 MHz sine waveform with a arbitrary waveform generator and a narrow bandwidth 150 MHz frequency filter. The peak frequency of the digitized frequency was determined with a FFT is (149.4 ± 1.0) MHz which is in agreement with the theoretical frequency of the sine waveform. Therefore it can be concluded that the GANDALFs sampling with the correct frequency of $880 \frac{\text{MS}}{\text{s}}$ and the external clock is working as intended. Also the GANDALF firmware was adjusted to trigger on positive input signals instead of negative pulses.

The most important settings of the eMUSIC boards were tested. The first of these was the measurement of the input offset voltage used to adjust the overvoltage of the SiPMs on a channel by channel level. It was found, that the input DAC, which sets the offset only follows a linear behavior between 100 DACu and 450 DACu. In this range the linear behavior measured with the eMUSIC board 2 is XXX and for the eMUSIC board 6 it is XXX. But the input offset differs between the different channels, therefore it is necessary to measure the input offset voltage while adjusting it. For both boards the input DACs were set to get approximatly 1 V input offset.

Also the pole-zero cancellation shaper was tested with different settings. Therefore measurements with deactivated pole-zero cancellation shaper were made as a reference. Also measurements with eight different settings for the shapers resistor at a constant setting for the shapers capacitor were done to see the effect of the resistor settings. In order to see the effect of the capacitor eight measurements with different capacitor settings but the same resistor setting were performed. The FWHM of the signals could be reduced down to a minimum of ns, depending on the pole-zero cancellation settings. But while the width decreased, the pole-zero cancellation shaper attenuated the signal amplitude down to . A % reduction compared to the amplitude without the pole-zero cancellation. In addition to the different pole-zero settings, also the lower attenuation option of the pole-zero cancellation shaper and the high transimpedance mode was tested.

Two dark count measurements were performed, one with and one without the pole-zero cancellation shaper. For the measurement with the pole-zero cancellation shaper, the resistor setting $R=3$ and the capacitor setting $C=31$ were chosen. In the histogram of the waveform integrals of both measurements no single photo-electron peaks could be distinguished. Hence it was not possible to use dark count measurements for calibration.

The eMUSIC board was successfully tested at the DESY testbeam and will be under a long time performens test starting in the near future.

Appendix A

List of acronyms

SM	Standard Model of particle physics
LHC	Large Hadron Colider
SHiP	Search for Hidden Particles
SPS	Super Proton Synchrotron
SBT	Surrounding Background Tagger
SiPM	Silicon Photomultiplier
PCB	Printed Circuit Board
ASIC	Application Specific Integrated Circuit
DAC	Digital to Analog Converter
ADC	Analog to Digital Converter
APD	Avalanche Photodiode
DAQ	Data Acquisition
WOM	Wavelength-shifting Optical Module
SPAD	Single Photon Avalanche Diode

DC	Dark Count
DCR	Dark Count Rate
FPGA	Field Programmable Gate Array
DESY	Deutsches Electronen SYnchrotron
eMUSIC	enhanced Multiple Use SiPM IC for photodetector readout
PMT	Photomultiplier tube
AMC	Analoge Mezzanine Card
OMC	Optical Mezzanine Card
DMC	Digital Mezzanine Card
NIM	Nuclear Instrumentation Module
HS	Hidden Sector
LAB	Linear Alkyl Benzene
FWHM	Full Width at Half Maximum
COMPASS	Common Muon Proton Apparatus for Structure and Spectroscopy
ENOB	Effective Number of Bits
PPO	Diphenyloxazole
GANDALF	Generic Advanced Numerical Device for Analytic and Logic Functions
FFT	Fast Fourier Transform

List of Figures

1.1	Overview of the SHiP experiment	4
1.2	Overview of the Surrounding Background Tagger	6
2.1	One Cell Prototype and PMMA vessel	8
2.2	LAB emission spectrum	9
2.3	Working principle of a WOM	10
2.4	Illustration of a APD.	12
2.5	eMUSIC block diagram	14
2.6	eMUSIC pole-zero cancellation	15
2.7	eMUSIC Board	18
2.8	Overview of the GANDALF module	20
2.9	Copper GIMLI	22
3.1	PCB with Hamamatsu SiPMs	24
3.2	Schematic view of the measurement setup.	26
3.3	Picture of the inside of the dark box.	27
4.1	FFT of a 150 MHz sin signal recorded with a GANDALF module. . .	30
4.2	Input offset measurement for eMUSIC board 2 channel 1	32
4.3	Input offset voltage of all channels for differen DAC settings	35
4.4	Mean waveform for a measurement without pole-zero cancellation. . .	38

4.5	Mean waveform for different pz-cancellation resistor values.	38
4.6	Mean waveform for different pz-cancellation capacitor values.	39
4.7	Plot of the low attenuation effect with two pole-zero settings.	42
4.8	Waveforms measured with low and high transimpedance	43
4.9	Histogram of the dark count measurements with pole-zero cancellation.	45
4.10	Histogram of the dark count measurements without pole-zero cancellation.	46
5.1	One Cell Prototype at the DESY testbeam	48

List of Tables

3.1	SiPM parameters	24
4.1	Input offset voltages fit	33
4.2	eMUSIC DAC settings for equal overvoltage between channels.	36
4.3	Amplitudes and FWHMs of measured signals for different PZ settings.	40

Bibliography

- [1] Y. F. et al., “Evidence for Oscillation of Atmospheric Neutrinos,” *Physical Review Letters*, vol. 81, pp. 1562–1567, aug 1998.
- [2] S. V. Troitsky, “Unsolved problems in particle physics,” *Physics-Uspekhi*, vol. 55, pp. 72–95, jan 2012.
- [3] SHiP Collaboration, “A facility to Search for Hidden Particles (SHiP) at the CERN SPS,” 2015.
- [4] A. Miano, A. Fiorillo, A. Salzano, A. Prota, and R. Jacobsson, “The structural design of the decay volume for the Search for Hidden Particles (SHIP) project,” *Archives of Civil and Mechanical Engineering*, vol. 21, 03 2021.
- [5] SHiP Collaboration, “SHiP Experiment - Comprehensive Design Study report,” tech. rep., CERN, Geneva, 2019.
- [6] F. Lyons, “Prototype WOM-based Liquid Scintillator Detector,” 09 2022.
- [7] SHiP Collaboration, “The SHiP experiment at the proposed CERN SPS Beam Dump Facility,” 2021.
- [8] J. Zimmermann, “Efficiency studies of a liquid-scintillator detector based on Wavelength-shifting Optical Modules,” Master’s thesis, 2020.
- [9] F. Acerbi and S. Gundacker, “Understanding and simulating SiPMs,” *Nuclear Instruments and Methods in Physics Research Section A: Accelerators, Spectrometers, Detectors and Associated Equipment*, vol. 926, pp. 16–35, 2019. Silicon Photomultipliers: Technology, Characterisation and Applications.

- [10] K. K. A. Ghassemi, K. Sato, “MPPC Literature,” 11 2022.
- [11] N. W. Hermann Kolanoski, *Teilchendetektoren Grundlagen und Anwendungen*. 2016.
- [12] J. Kemp, *Development of a silicon photomultiplier based scintillator detector for cosmic air showers*. Dissertation, RWTH Aachen University, Aachen, 2020. Veröffentlicht auf dem Publikationsserver der RWTH Aachen University 2021; Dissertation, RWTH Aachen University, 2020.
- [13] Hamamatsu, “MPPC Technical note.”
- [14] Scientifica, *eMUSIC Datasheet*.
- [15] S. Gómez, D. Sánchez, J. Mauricio, E. Picatoste, A. Sanuy, A. Sanmukh, M. Ribó, and D. Gascón, “Multiple Use SiPM Integrated Circuit (MUSIC) for Large Area and High Performance Sensors,” *Electronics*, vol. 10, no. 8, 2021.
- [16] F. Herrmann, *Development and verification of a high performance electronic readout framework for high energy physics*. PhD thesis, 2011.
- [17] Hamamatsu, “Hamamatsu MPPC S14160/S14161 series Datasheet.”
- [18] Onsemi, “Silicon Photomultipliers (SiPM), High PDE and Timing Resolution Sensors in a TSV Package, J-Series SiPM sensors Datasheet,” 08 2021.
- [19] Thorlabs, “Thorlabs BKF12, Black Aluminum Foil.”
- [20] A. Bismark, “LED Calibration System with Optical Fibers for a LXe TPC,” 2017.

Erklärung

Hiermit versichere ich, dass ich die eingereichte Masterarbeit selbständig verfasst habe. Ich habe keine anderen als die angegebenen Quellen und Hilfsmittel benutzt und alle wörtlich oder sinngemäß aus anderen Werken übernommenen Inhalte als solche kenntlich gemacht. Weiter versichere ich, dass die eingereichte Masterarbeit weder vollständig noch in wesentlichen Teilen Gegenstand eines anderen Prüfungsverfahrens war oder ist.
